ADVANCED HEALTHCARE MATERIALS
www.advhealthmat.de

Lung-Mimetic Hydrofoam Sealant to Treat Pulmonary Air Leak

Meghan R. Pinezich, Mohammad Mir, Pamela L. Graney, Daniel Naveed Tavakol, Jiawen Chen, Maria R. Hudock, Olimpia Gavaudan, Panpan Chen, Sarah R. Kaslow, Jonathan A. Reimer, Julie Van Hassel, Brandon A. Guenthart, John D. O'Neill, Matthew Bacchetta, Jinho Kim, and Gordana Vunjak-Novakovic**

Pulmonary air leak is the most common complication of lung surgery, contributing to post-operative morbidity in up to 60% of patients; yet, there is no reliable treatment. Available surgical sealants do not match the demanding deformation mechanics of lung tissue; and therefore, fail to seal air leak. To address this therapeutic gap, a sealant with structural and mechanical similarity to subpleural lung is designed, developed, and systematically evaluated. This "lung-mimetic" sealant is a hydrofoam material that has alveolar-like porous ultrastructure, lung-like viscoelastic properties (adhesive, compressive, tensile), and lung extracellular matrix-derived signals (matrikines) to support tissue repair. In biocompatibility testing, the lung-mimetic sealant shows minimal cytotoxicity and immunogenicity in vitro. Human primary monocytes exposed to sealant matrikines in vitro upregulate key genes (MARCO, PDGFB, VEGF) known to correlate with pleural wound healing and tissue repair in vivo. In rat and swine models of pulmonary air leak, this lung-mimetic sealant rapidly seals air leak and restores baseline lung mechanics. Altogether, these data indicate that the lung-mimetic sealant can effectively seal pulmonary air leak and promote a favorable cellular response in vitro.

1. Introduction

Pulmonary air leak is the most common complication of lung surgery, presenting in up to 60% of patients after surgery.[1] Despite high prevalence, there are no consensus guidelines on post-operative air leak management, and treatment strategies vary by institution and practitioner. Chest tube drainage systems are often used to manage pneumothorax while the air leak is allowed to resolve on its own. However, air leak can persist for days to weeks, contributing to post-operative complications, including infection.[1]

Conventional air leak treatment options (e.g., pleurodesis, pleural tenting, and endobronchial valves) have significant shortcomings and do not definitively improve outcomes.[2] Pleurodesis and pleural tenting utilize chemical injury and anastomosis, respectively, to adhere the visceral pleura to the chest wall and prevent pneumothorax. However, both methods can

M. R. Pinezich, P. L. Graney, D. N. Tavakol, M. R. Hudock, O. Gavaudan, P. Chen, S. R. Kaslow, J. A. Reimer, J. Van Hassel, G. Vunjak-Novakovic
Department of Biomedical Engineering
Columbia University
New York 10027, USA
E-mail: gv2131@columbia.edu

M. Mir, J. Chen, J. Kim
Department of Biomedical Engineering
Stevens Institute of Technology
Hoboken, New Jersey 07030, USA
E-mail: jkim6@stevens.edu

P. Chen, S. R. Kaslow, J. A. Reimer, J. Van Hassel
Department of Surgery
Columbia University Irving Medical Center
New York 10032, USA

B. A. Guenthart
Department of Cardiothoracic Surgery
Stanford University
Stanford, California 94304, USA

J. D. O'Neill
Department of Cell Biology
State University of New York Downstate Medical Center
Brooklyn, New York 11226, USA

M. Bacchetta
Department of Thoracic Surgery
Vanderbilt University Medical Center
Vanderbilt University
Nashville, Tennessee 37232, USA

M. Bacchetta
Department of Biomedical Engineering
Vanderbilt University
Nashville, Tennessee 37203, USA

G. Vunjak-Novakovic
Columbia University Irving Medical Center
Department of Medicine
New York 10032, USA

The ORCID identification number(s) for the author(s) of this article can be found under https://doi.org/10.1002/adhm.202303026

DOI: 10.1002/adhm.202303026

Table 1. Key design criteria for lung-mimetic sealant.

Criteria	Parameter	Specification
Alveolar-like aerated pores	Pore diameter	200 ± 100 µm
Lung-like deformation mechanics	Extensibility	125% ± 25%
Pleural-like strength	Burst pressure	>50 cm H_2O
Strong adhesion to lung	Adhesion strength	>4900 N m^{-3}
Rapid curing on lung surface	Gelation time	<60 s
Biocompatibility	Cell viability	>90%
Biodegradability	Degradation time	<14 days
Favorable cellular response	Expression of repair genes	Yes

cause fibrosis and scarring in the treated region[3] and correlate with further post-operative complications.[4,5] Endobronchial valves, which are used to prevent airflow to the site of air leak, cause regional atelectasis that hinders healing.[6] In rare cases, surgical intervention may be required for patients with severe, persistent air leak (e.g., bronchopleural fistula), or for patients who have underlying lung disease (e.g., chronic obstructive pulmonary disease (COPD), emphysema) with aberrant wound healing and high risk of spontaneous pneumothorax.[7]

One promising approach to treat post-operative pulmonary air leak is the application of a surgical sealant to the site of air leak. Although many surgical sealants have been investigated, none has demonstrated the ability to resolve pulmonary air leak; and thus, no sealant is widely used. Progel, the only surgical sealant approved for application to the visceral pleura to treat visible air leaks incurred during resection of lung parenchyma, fails in up to 65% of applications and is not associated with decreased incidence of post-operative air leak.[8] Available surgical sealants intended for other indications (e.g., BioGlue, Evicel, and TISSEEL) are sometimes used off-label to treat air leak but are ineffective due to poor adhesion or insufficient physicomechanical properties that are mismatched with the surrounding lung tissue (Table S1, Supporting Information).[8–20] A surgical sealant that effectively seals air leak and promotes tissue repair has the potential to significantly reduce post-operative burden, risk of complications, hospital length of stay, and/or healthcare costs currently associated with management of air leak.

To address this therapeutic gap, we define key design criteria for an effective lung sealant (**Table 1**), then develop and systematically evaluate a sealant with structural and mechanical similarity to subpleural lung. Here, we report the design and characterization of our "lung-mimetic" sealant, a hydrofoam material that has: i) alveolar-like porous ultrastructure, ii) lung-like viscoelastic properties (adhesive, compressive, tensile), and iii) lung extracellular matrix-derived signals (matrikines) to support tissue repair (**Figure 1**). Accordingly, we test an array of sealant formulations to ensure design criteria are satisfied, validate sealant biocompatibility with human primary lung fibroblasts and monocytes, and demonstrate sealant efficacy in rat and swine models of pulmonary air leak induced by focal punctures similar to those resulting from intraoperative tissue manipulation or surgical stapler misfire.

2. Results

We developed a lung-mimetic sealant comprised of gelatin (structural biopolymer), tannic acid (tissue adhesion promotor), transglutaminase (crosslinking initiator), and lung extracellular matrix-derived matrikines (tissue repair promoter) (Figure 1A). As available surgical sealants fail due to physicomechanical properties that are mismatched with surrounding lung tissue, we designed the sealant to mimic, and therefore, better match key structural and mechanical properties of lung (Figure 1B). When applied to the visceral pleura at the site of air leak, the sealant adhered to the pleura and rapidly sealed the air leak (Figure 1C,D). In this study, we characterized physicomechanical properties of the lung-mimetic sealant, compared against the corresponding structural and mechanical properties of lung tissue and demonstrated sealant efficacy in rat and swine models of pulmonary air leak.

2.1. Lung-Mimetic Sealant Formulation and Physical Properties

To modulate the physical characteristics of the lung-mimetic sealant, we incorporated gelatin, tannic acid, and transglutaminase into the sealant formulation (**Figure 2A**). Gelatin is a hydrolyzed form of collagen, which is the primary structural protein in lung extracellular matrix.[21] Tannic acid binds gelatin through a one-step Michael addition reaction in oxidizing conditions, enabling strong adhesion to a wet tissue surface.[22,23] Tannic acid may also offer benefits due to its antioxidant and antimicrobial properties.[24] Transglutaminase is an enzymatic crosslinking initiator that catalyzes formation of a covalent isopeptide bond between the ϵ-amino group of lysine and the γ-carboxamide group of glutamine in gelatin, enhancing mechanical integrity, thermal stability, and integration with underlying lung tissue (Figure 2B).[25,26] To mimic the ultrastructure of aerated lung tissue, we introduced micro-sized air bubbles to the sealant before crosslinking (Figure 2C; Figure S1A, Supporting Information). We modulated air bubble size and density by controlling the rotational speed of the mixer and generated aerated pores that resembled alveolar structure and had an average diameter similar to human lung alveoli (lung-mimetic sealant: 208 ± 84.4 µm; human lung: 225 ± 39.2 µm, $p = 0.1$), as shown by scanning electron microscopy (Figure 2D; Figure S1B, Supporting Information). Pore size was not significantly affected by the range of matrikine concentrations in this study (Figure S2, Supporting Information).

2.2. Lung-Mimetic Sealant Mechanical and Biochemical Properties

2.2.1. Compression and Tension

We measured the mechanical properties of sealant formulations across a range of transglutaminase concentrations (0%, 1%, 2%, 4%, w/v) using standardized compression and tension testing. The stress–strain curve from compression testing showed nonlinear viscoelastic behavior for all sealant formulations (**Figure 3A**). We determined compression moduli at three strain ranges: low (0–0.05), medium (0.30–0.35), and high (0.45–0.50). Similar to lung and other soft tissues, sealant compression

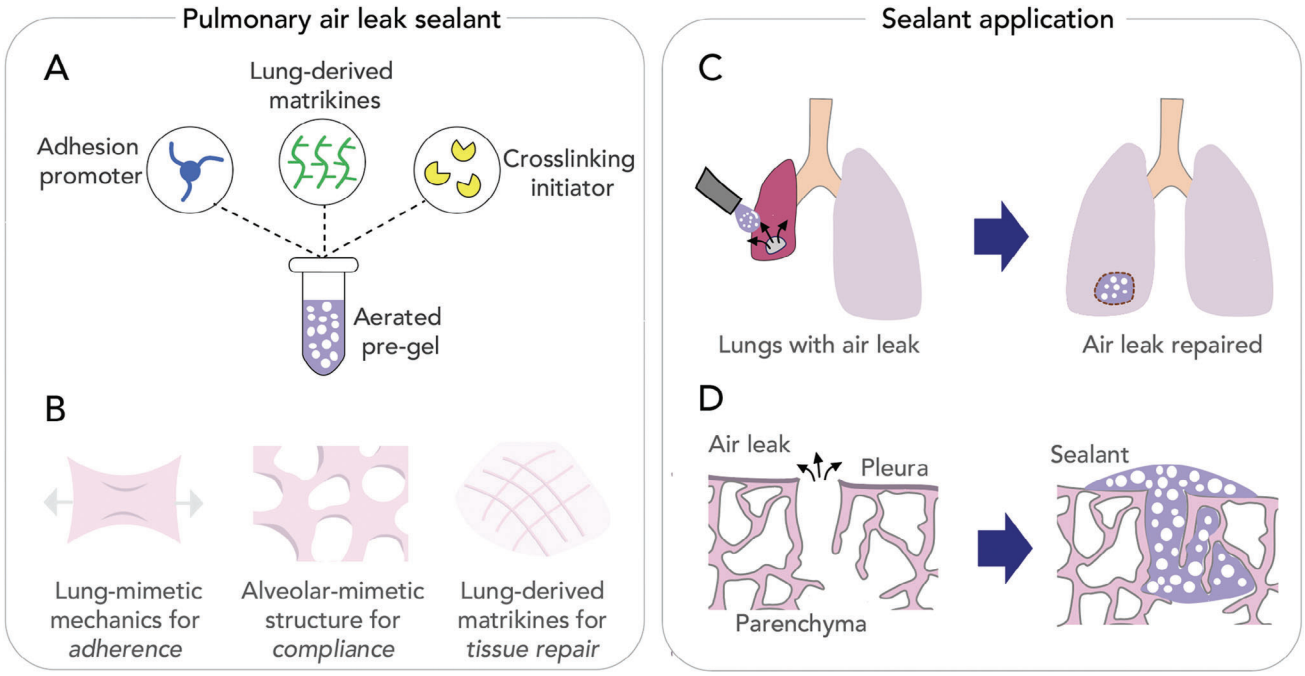

Figure 1. Overview of lung-mimetic hydrofoam sealant to treat pulmonary air leak. A) Sealant is formulated with an adhesion promoter (tannic acid), lung-derived matrikines, and a crosslinking initiator (transglutaminase). B) Sealant features lung-mimetic mechanics to ensure adherence, alveolar-mimetic structure for compliance similar to lung tissue, and lung-derived matrikines to promote tissue repair. C) Sealant is applied to the visceral pleura at the site of air leak, rapidly sealing the air leak and restoring baseline lung mechanics. D) Cross-sectional view of sealant application.

moduli increased nonlinearly with increasing strain.[27] Further, increasing transglutaminase concentration resulted in greater sealant compression moduli across all strain ranges (Figure 3B). To determine Young's modulus and elongation at failure under stretch conditions similar to those the sealant encounters during the respiratory cycle, we performed tension testing (Figure 3C; Figure S3, Supporting Information). Young's moduli for sealant formulations with 0%, 1%, 2%, and 4% w/v transglutaminase were: 12.0 ± 3.0 kPa, 18.6 ± 1.5 kPa, 25.7 ± 1.3 kPa, and 33.9 + 3.8 kPa, respectively (Figure 3D). Elongation at failure for sealant formulations with 0%, 1%, 2%, and 4% w/v transglutaminase was: 40.0% ± 6.8%, 169.6% ± 11.3%, 124.8% ± 14.3%, and 92.2% ± 11.0%, respectively (Figure 3E). Sealant toughness was determined by calculating the area under the stress–strain curve of elongation to failure measurements (Figure S3A, Supporting Information). Toughness values for sealant formulations with 0%, 1%, 2%, and 4% w/v transglutaminase were: 1.01, 15.4, 27.5, and 31.5 kJ m^{-3}, respectively (Figure S3B, Supporting Information). Neither Young's modulus nor elongation at failure was significantly affected by the range of matrikine concentrations in this study (Figure S4, Supporting Information).

2.2.2. Adhesion

We measured the adhesive properties of sealant formulations using a customized force measurement system (Figure 3F–H). As tannic acid was used as a tissue adhesion promotor, we investigated adhesion strength as a function of tannic acid concentration. For sealant formulations with 0%, 0.01%, 0.1%, 0.5%, and 1% w/v tannic acid, the magnitude of force required to detach the sealant from a test substrate was: 0.32 ± 0.10 N, 1.35 ± 0.72 N, 2.42 ± 0.72 N, 0.71 ± 0.31 N, and 0.28 ± 0.12 N, respectively (Figure 3I).

2.2.3. Thermal Stability at Physiological Temperature

As the lung sealant is deployed at body temperature, we investigated whether the structural integrity of the sealant could be maintained at 37 °C. Notably, sealant formulations that were crosslinked with transglutaminase remained intact and thermally stable at 37 °C, whereas, sealant formulations that were not crosslinked with transglutaminase melted rapidly (Video S1, Supporting Information).

2.2.4. Proteomic Profile

We characterized the lung extracellular matrix-derived matrikines by performing liquid chromatography–tandem mass spectrometry (LC–MS/MS) and multiplex protein profiling. Matrikines derived from decellularized lung extracellular matrix including collagens (collagen I, II, III, IV, V, VI, VIII, IX, XI, and XVI), glycoproteins (elastin, fibrillin-1, fibulin-5, laminin, nidogen, and periostin), and proteoglycans (aggrecan, heparan sulfate, and hyaluronan) were identified.[28] Several endogenous growth factors, including amphiregulin, basic fibroblast growth factor (bFGF), bone morphogenetic protein 5 (BMP-5), bone morphogenetic protein 7 (BMP-7), hepatocyte growth factor (HGF), and insulin-like growth factor binding proteins, were also identified. The proteomic profile of our lung-mimetic sealant is

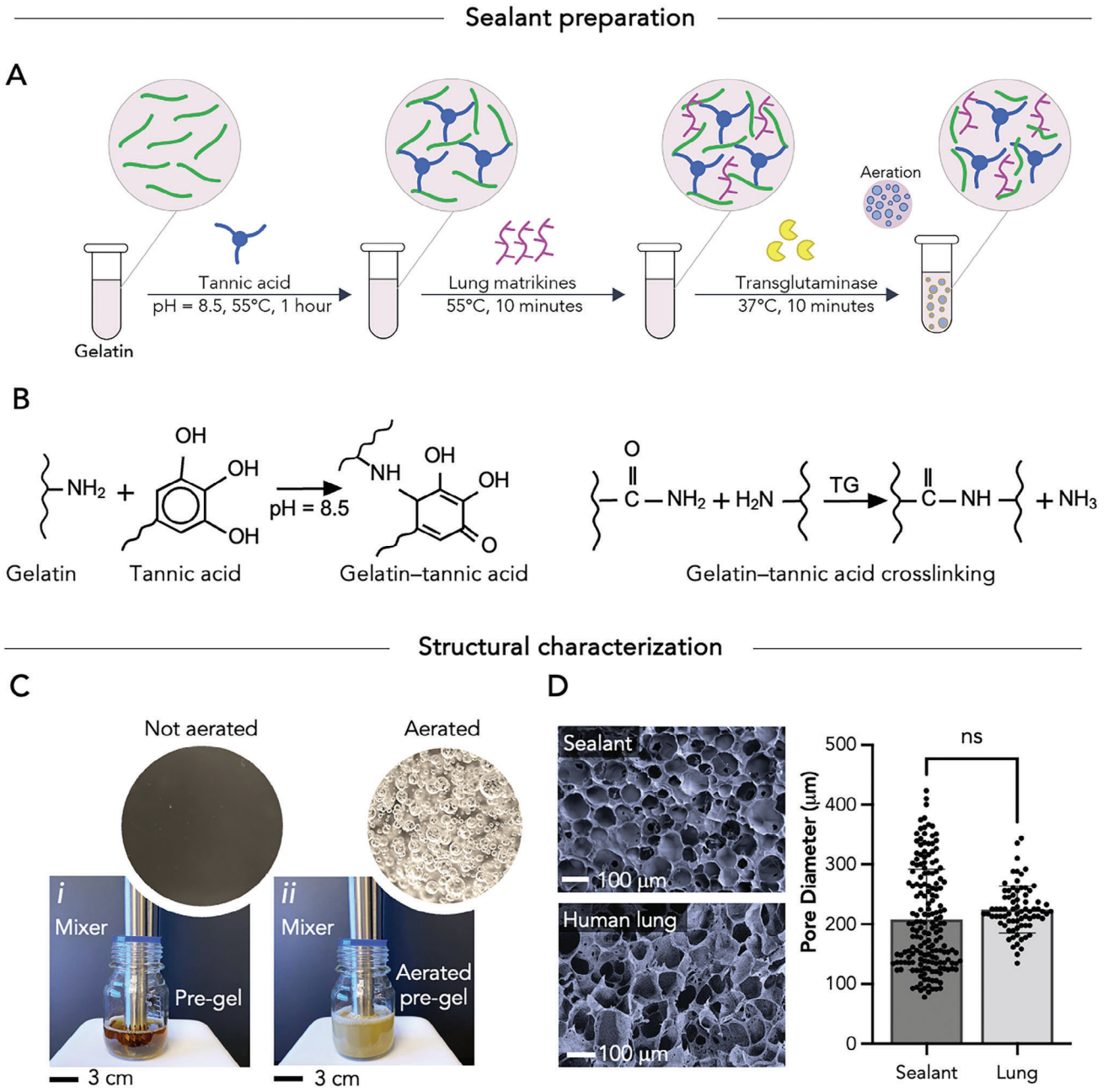

Figure 2. Preparation and structural characterization of lung-mimetic sealant. A) Sealant preparation process. Tannic acid is added to gelatin solution at 55 °C, and the resulting solution is mixed for 1 h at pH = 8.5. Lung-derived matrikines are added to the gelatin–tannic acid solution, and the resulting solution is mixed for 10 min at 55 °C. Transglutaminase is added to the gelatin–tannic acid–lung matrikine solution at 37 °C, and the final solution is mixed for 10 min before application. B) Chemical reaction between gelatin and tannic acid and crosslinking via transglutaminase. C) Photographs of pre-gel: C-i) before aeration and C-ii) after aeration. D) Scanning electron microscopy of lung-mimetic sealant and human lung, with corresponding quantification of pore diameter ($p = 0.1$; ns, not significant). TG, transglutaminase.

described in detail in Table S2, Supporting Information, including a brief description of each factor identified.[29–66]

2.2.5. Cytotoxicity

Evaluation of cytotoxicity is a significant biological endpoint required for regulatory approval of implantable materials. We evaluated potential cytotoxicity of sealant formulations across a range of matrikine concentrations (10% gelatin; 2% transglutaminase; 0%, 0.01%, 0.05%, 0.1%, and 0.2% w/v matrikines). Human primary lung fibroblasts were used as a representative cell type, as fibroblasts would be in direct contact with the sealant in clinical use. To qualitatively evaluate the potential of sealant formulations to cause cell death, we performed live/dead staining and imaging. Lung fibroblasts maintained high viability (>95%) and

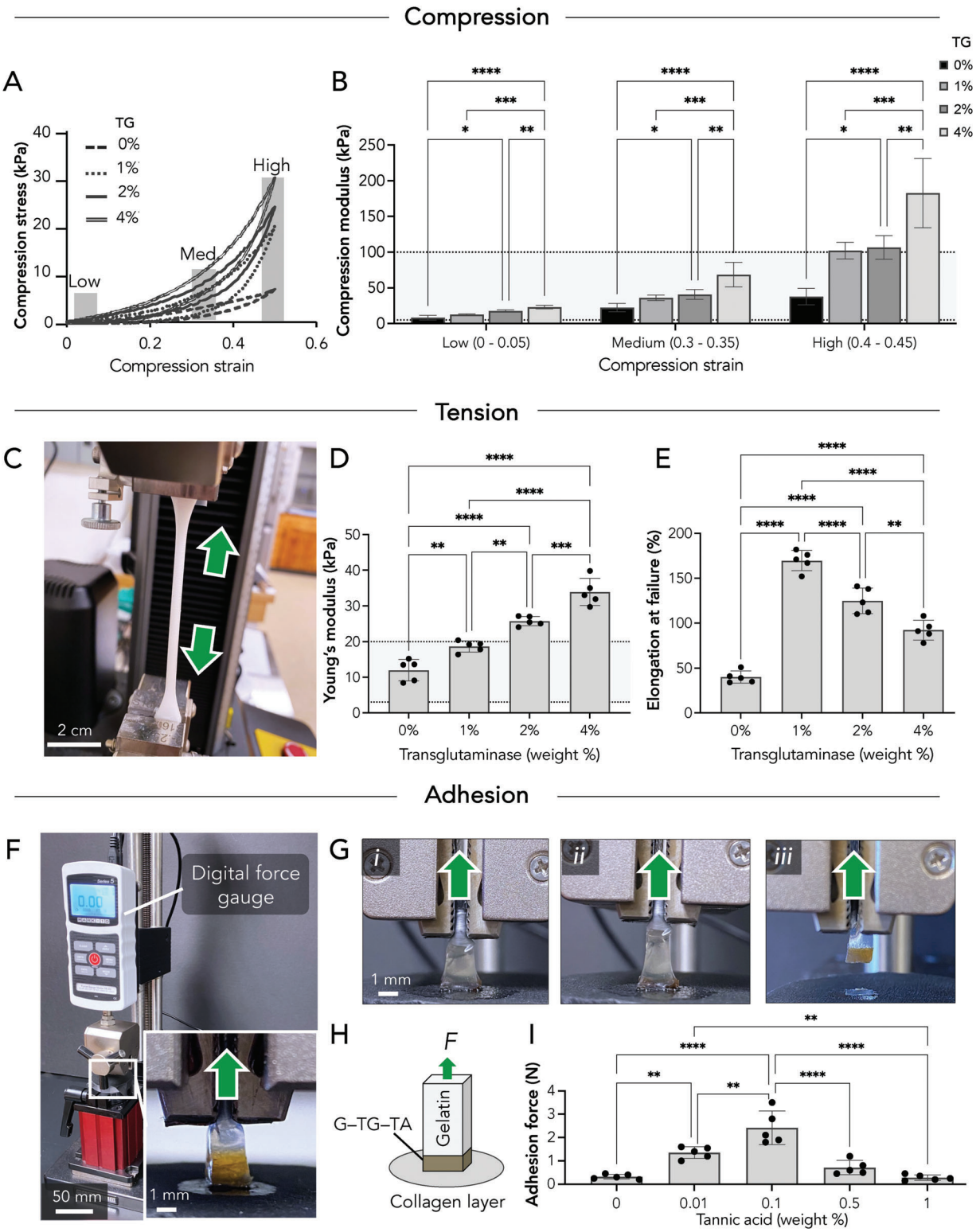

Figure 3. Mechanical and adhesion characterization of lung-mimetic sealant. A) Stress–strain curve of compression test for sealant formulations across a range of transglutaminase concentrations. B) Elastic modulus of sealant formulations across different strain ranges. Shaded region indicates range of elastic modulus in human lungs. C) Setup for tension testing of sealant. D) Young's modulus and E) elongation at failure values of sealant formulations across a range of transglutaminase concentrations. Shaded region indicates range of Young's modulus in human lungs. F) Setup for adhesion testing of sealant formulations across a range of tannic acid concentrations. G) Photographic sequence of sealant detaching from collagen layer under increasing tension. H) Schematic of adhesion testing. I) Calculated adhesion force of sealant formulations across a range of tannic acid concentrations. F, force; G, gelatin; TA, tannic acid; TG, transglutaminase. *$p < 0.05$, **$p < 0.01$, ***$p < 0.001$, and ****$p < 0.0001$.

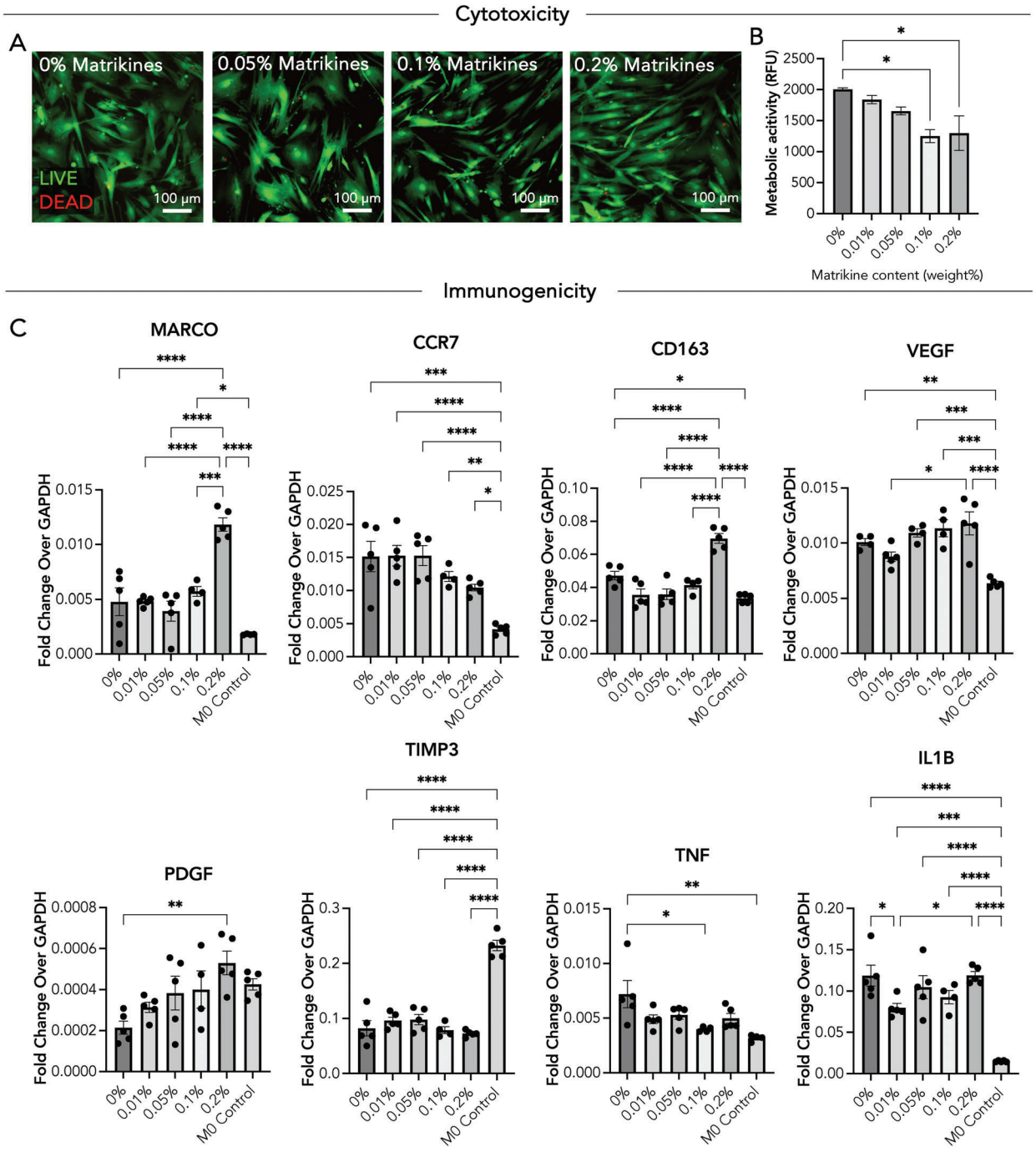

Figure 4. Biocompatibility of lung-mimetic sealant. A) Representative cell viability staining of human primary lung fibroblasts in response to a range of lung matrikine concentrations (0–0.2%). Green, live cells; red, dead cells. B) Metabolic activity of human primary lung fibroblasts in response to a range of lung matrikine concentrations (0–0.2%). C) Relative gene expression of human primary monocytes in response to a range of lung ECM concentrations (0–0.2%). *$p < 0.05$, **$p < 0.01$, ***$p < 0.001$, and ****$p < 0.0001$.

normal fibroblastic morphology across all matrikine concentrations, and minimal/no cell death was observed (**Figure** 4A). To quantitatively evaluate the potential of the sealant to inhibit cell growth, we performed a fluorometric cell viability assay. Reduction of metabolic activity greater than 50% would raise concern for cytotoxicity. In this study, increasing matrikine concentration correlated with reduction of metabolic activity by ≈10–35%, an acceptable and expected response consistent with other studies investigating biocompatibility of matrikines in vitro (Figure 4B).

2.2.6. Immunogenicity

We evaluated immunogenicity, the potential to generate an immune response, of sealant formulations across a range of

matrikine concentrations (10% gelatin; 2% transglutaminase; 0%, 0.01%, 0.05%, 0.1%, and 0.2% w/v matrikines). Human primary monocytes were used to assess in vitro immunogenicity, including effects of the sealant on expression of key inflammatory markers. Use of primary human monocytes to assess in vitro immunogenicity is standard for pre-clinical evaluation of implantable materials[67] and offers the advantage of using human primary immune cells to predict the nature of immunological interactions in clinical application. In the lung, wound healing and tissue repair are mediated by multiple cell types, including monocytes, which can differentiate into macrophages with pro-inflammatory or pro-reparative phenotypes. Human primary monocytes were exposed to a range of matrikine concentrations in a transwell co-culture system, and gene expression of CCR7, CD163, IL1B, MARCO, PDGF, TIMP3, TNF, and VEGF, was analyzed after 3 days. Across the panel of inflammatory markers investigated, no order-of-magnitude changes in gene expression were observed, suggesting overall low immunogenic effect of the sealant on human monocytes. All sealant formulations showed a minimal but expected increase in expression of inflammatory markers CCR7, IL1B, and TNF compared to control (isolated M0 monocytes) (Figure 4C).

Although upregulated compared to control, CCR7 expression decreased with increasing matrikine concentration, suggesting that matrikines modulate inflammatory response. TNF expression was similarly elevated compared to control, but showed no significant changes in response to altered matrikine concentration. The only significant difference in VEGF expression was a 1.4-fold increase between 0.01% and 0.2% matrikines ($p < 0.05$). IL1B expression showed the same pattern, with the only significant difference between 0.01% and 0.2% matrikines ($p < 0.05$). Notably, matrikines have also been shown to promote a favorable cellular response by regulating expression of genes that correlate with tissue repair.[68] With increasing concentration of matrikines, monocytes increased expression of markers of extracellular matrix remodeling and M2 anti-inflammatory macrophages, including CD163 and MARCO, which were both expressed at significantly higher levels in monocytes exposed to 0.2% matrikines. Expression of MMP9, another marker of ECM remodeling, also trended upward compared to control, but the difference was not significant. Expression of TIMP3 was significantly downregulated across all matrikine concentrations compared to control, and no significant difference was observed between matrikine concentrations (Figure 4C).

2.3. Lung-Mimetic Sealant Efficacy At Treating Air Leak

2.3.1. Efficacy in Rat Model of Pulmonary Air Leak

We evaluated sealant efficacy in a rat model of pulmonary air leak (**Figure 5A**; Video S2, Supporting Information). To induce air leak, an incision (2 cm) was made in the lung, and subsequently, airway pressure (P_{airway}) significantly decreased (Figure 5B-i-iii,C). Normal saline was added to the incision, and air bubbles were observed, confirming presence of air leak (Video S3, Supporting Information). When lung-mimetic sealant was topically applied to the visceral pleura at the site of air leak, airway pressure was rapidly restored to baseline (Figure 5B-iv,C), and no air bubbles were observed (Video S4, Supporting Information), indicating an effective seal of the air leak. After inducing air leak, peak inspiratory pressure (PIP) decreased from 18.8 ± 0.2 cm H_2O to 13.4 ± 0.3 cm H_2O ($p < 0.001$, baseline vs air leak). After applying sealant, PIP increased from 13.4 ± 0.3 cm H_2O to 18.7 ± 0.4 cm H_2O ($p < 0.001$, air leak vs sealant) (Figure 5D). No significant difference in PIP was observed between lungs at baseline and lungs treated with sealant ($p = 0.39$). Loss of inspiratory volume (volume loss) was measured by calculating the area under the flow–time curve during inhalation (V_I) and exhalation (V_E) at baseline, air leak, and sealant application. Volume loss increased from 8% ± 2% to 67% ± 2% ($p < 0.001$) at induction of air leak but returned to 8% ± 4% ($p < 0.001$) when lung-mimetic sealant was applied (Figure 5E). No significant difference in volume loss was observed between lungs at baseline and lungs treated with sealant ($p = 0.89$). Notably, the pressure–volume loop showed recovery of dynamic compliance after sealant application (Figure 5F). Representative scanning electron microscopy showed sealant integration into the underlying lung tissue (Figure 5G-i). Lung-mimetic sealant proximal to the site of air leak also integrated into the underlying lung tissue (Figure 5G-ii), which correlated with rapid recovery of peak inspiratory pressure. The sealant remained localized to the subpleural region and was not observed in parenchymal regions significantly beyond the site of air leak (Figure 5G-iii).

2.3.2. Efficacy in Ex Vivo Swine Lungs

We evaluated sealant efficacy in a swine model of pulmonary air leak. Swine lungs were used to evaluate sealant efficacy due to similarities in ventilation parameters (airway pressure and tidal volume) and pleural composition to those of human lungs (**Figure 6A**). Air leak was induced by a focal pleural puncture. Lungs with air leak were submerged in normal saline, and visualization of air bubbles confirmed the presence of air leak (Figure 6B; Video S5, Supporting Information). After sealant application, no bubbles were visible when the lungs were submerged in saline (Figure 6C; Video S6, Supporting Information). Induction of air leak led to a significant decrease in tidal volume to 17.3% ± 13.5% ($p < 0.05$), which was restored to near baseline after sealant application (baseline: 4.38% ± 2.3%, sealant: 2.90% ± 4.5%, $p = 0.94$) (Figure 6D). Notably, lung-mimetic sealant rapidly adhered to the visceral pleura and successfully sealed air leak within 60 s of application, a timeframe confirmed acceptable by practicing thoracic surgeons. Histological analysis of the applied sealant showed robust integration of the sealant with the surrounding lung tissue at the site of air leak (Figure 6E). We also performed a sound-based air leak detection test established by our group, wherein the intensity and frequency of air leak sounds were analyzed to quantify severity of air leak.[69] We found that after induction of air leak, sound pressure levels were significantly elevated relative to baseline (baseline: 7.86 ± 0.11 dBA, air leak: 49.4 ± 20.8 dBA, $p < 0.05$). After sealant application; however, sound pressure levels showed no significant difference compared to baseline levels (sealant: 10.2 ± 3.0 dBA, $p = 0.893$) (Figure 6F). Similarly, after sealant application, the frequency profiles of air leak sounds also returned to baseline (Figure 6G).

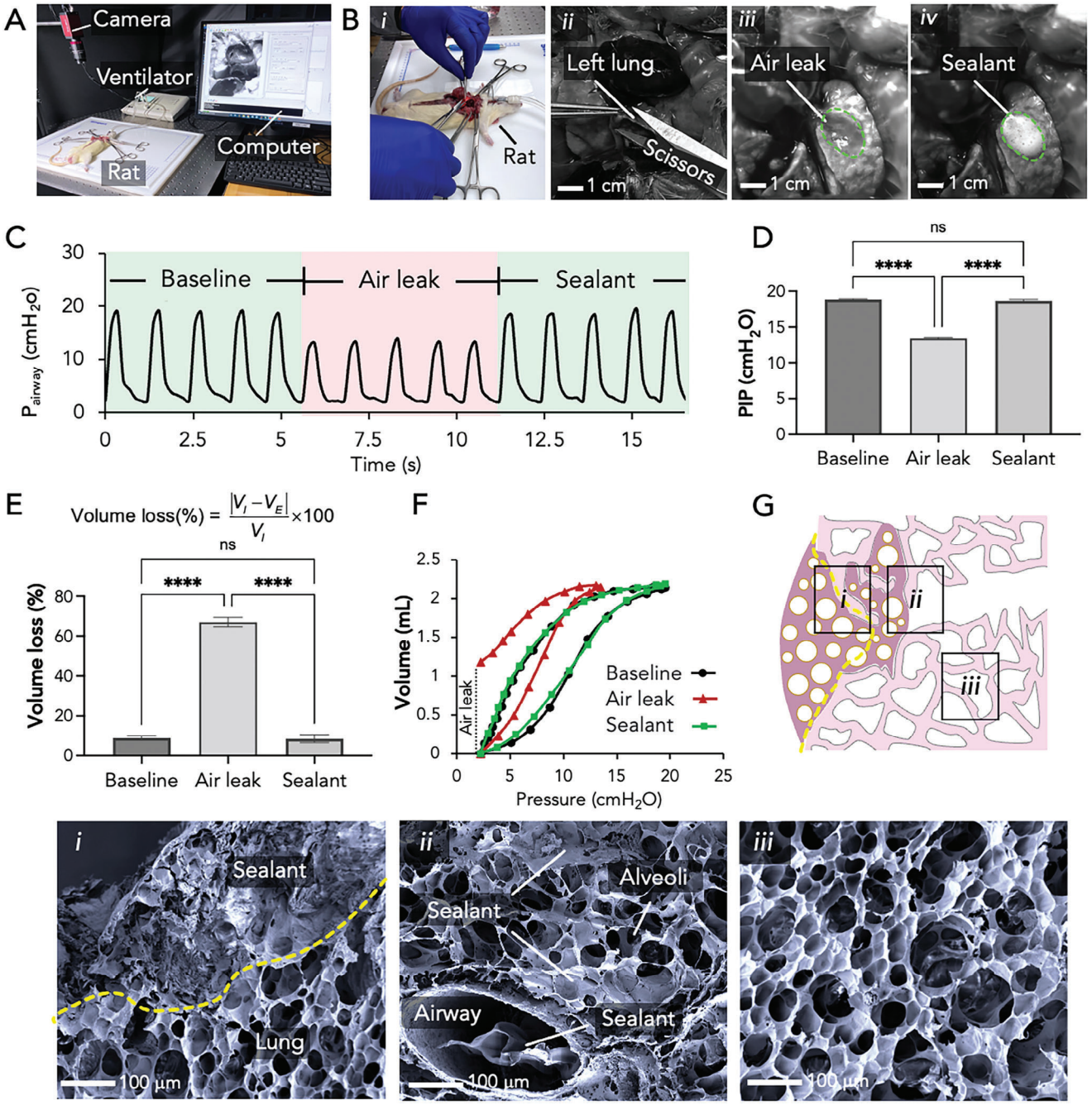

Figure 5. Efficacy of lung-mimetic sealant in rat model of pulmonary air leak. A) Experimental setup for monitoring rat lungs before and after sealant application. B) Representative photographs of air leak induction: B-i) preparation of rat, B-ii) 2-cm incision in left lung, B-iii) air leak, and B-iv) sealant application. C) Continuously monitored airway pressure at baseline, air leak, and sealant application. D) Peak inspiratory pressure (PIP) at baseline, air leak, and sealant application. E) Volume loss during inspiration/expiration at baseline, air leak, and sealant application. F) Pressure–volume loops at baseline, air leak, and sealant application. G) Scanning electron microscopy: G-i) sealant integration with visceral pleura (dotted line) at air leak site, G-ii) sealant in alveoli adjacent to air leak site, G-iii) alveoli in unaffected area proximal to air leak site. V_I: volume of inspiration, V_E, volume of expiration. ns, not significant and ****$p < 0.001$.

3. Discussion

Mechanical properties of the lung arise from the interdependent architecture of the alveolar network, pulmonary surfactant that reduces alveolar surface tension, and a highly complex extracellular matrix network capable of stretch and elastic recoil.[70] Immediately following air leak, intrinsic lung tissue mechanics and mechanobiology are compromised with the loss of pleural integrity, poor ventilation, and localized atelectasis and edema. An ideal lung sealant must rapidly restore normal lung mechanics

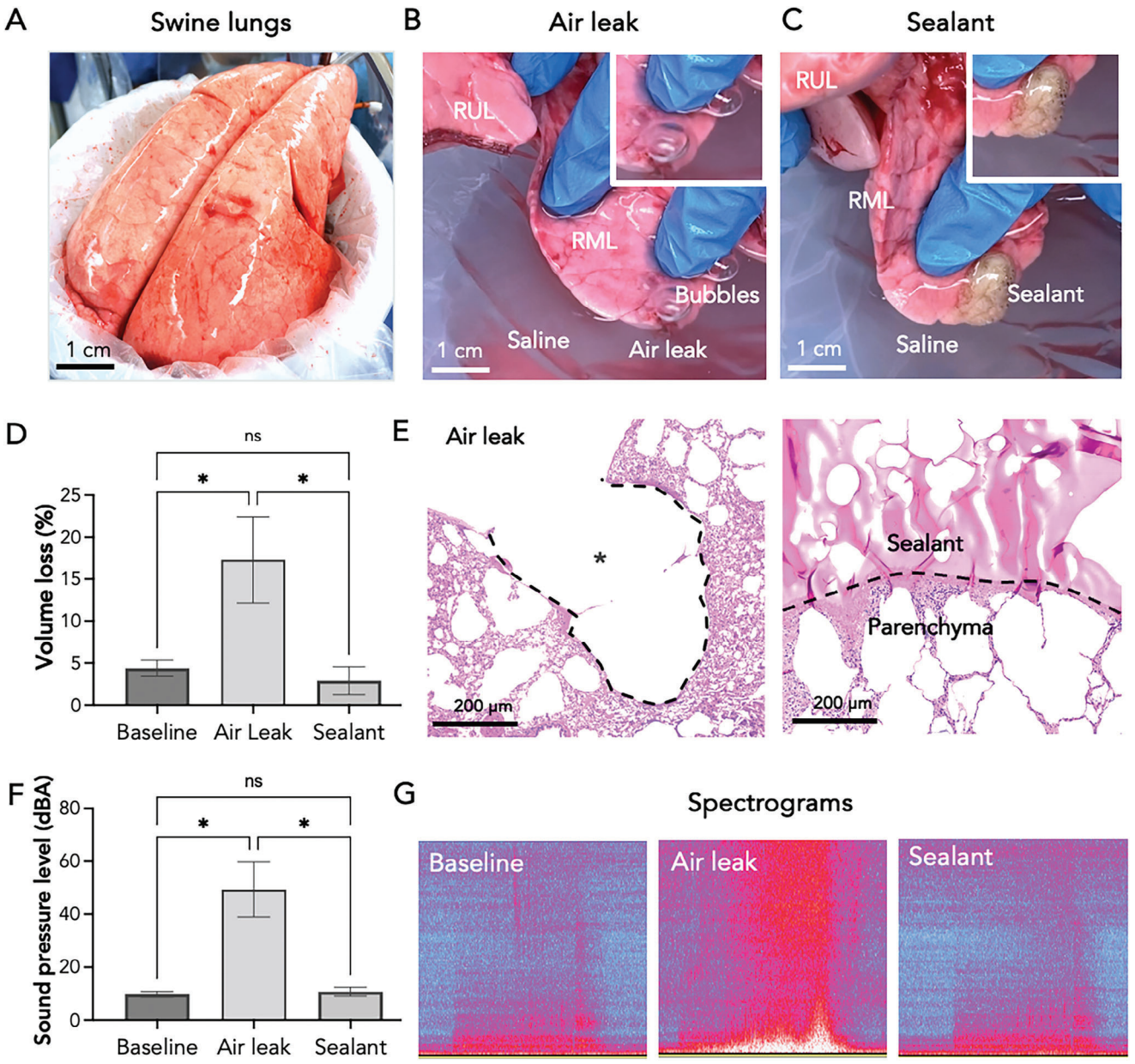

Figure 6. Efficacy of lung-mimetic sealant in ex vivo swine lungs. Representative photographs of: A) Ex vivo swine lungs. B) Site of air leak in right middle lobe. Visible bubbles confirmed presence of air leak. C) After sealant application, no bubbles were observed. D) Sealant application reduced volume loss and restored baseline tidal volume. E) Histologic micrographs: site of air leak before (left) and after (right) sealant application. Sealant maintained robust adhesion to the visceral pleura (dotted line). F) Sound pressure level significantly increased after air leak induction and returned to baseline after sealant application. G) Representative spectrograms: sealant application restored the spectrogram to baseline. RUL, right upper lobe. RML, right middle lobe. dBA, A-weighted decibels. ns, not significant. *$p < 0.05$.

and promote repair of damaged tissue. Based on the principle that the structural interdependence of alveoli enables uniform expansion during inspiration and prevents atelectasis (collapse) during expiration, we describe the first sealant with an alveolar-like structure. We observe that an alveolar-like structure confers key mechanical properties, for example, nonlinear viscoelastic behavior, that are well-matched to the lung, enabling the sealant to expand uniformly and repeatably with cyclic deformation of the lung during ventilation.

The visceral pleura is primarily comprised of a collagen and elastin network that directly integrates with the elastic fibers of adjacent alveolar walls in the lung parenchyma, enabling the distal lung to function as a single mechanical unit. Within the visceral pleura is a thin layer of mesothelial cells that serves as an interface between the lung parenchyma and the intrapleural space, which is filled with fluid to lubricate the surface of the lung during ventilation.[71–73] An aberrant cellular response to a focal or diffuse pleural injury can cause pleuritis or adhesions

between the visceral pleura and the chest wall,[30] which may lead to further inflammation, post-surgical complications, and technical difficulties if reoperation is needed.[74,75] The lung-mimetic sealant is designed to both address the mechanical failure of air leak and promote pleural tissue repair. Thus, we formulate the lung-mimetic sealant with gelatin (structural biopolymer), transglutaminase (crosslinking initiator), tannic acid (tissue adhesion promoter), and lung-derived matrikines (tissue repair promoter).

Although tannic acid serves as a tissue adhesion promoter, we observe that sealant adhesion decreases above 0.1% tannic acid. The reason for this trend is not immediately clear, though others in the field report similar observations. We suspect that sealant formulations with tannic acid concentration above 0.1% may decrease adhesion because available gelatin side groups are consumed in the oxidation of tannic acid at higher concentrations.[76–78] Notably, adhesive and mechanical properties necessary for effective sealing of air leak may differ regionally, temporally, and from patient to patient depending on underlying tissue damage and/or disease. Mechanical ventilation during or immediately after lung surgery may place additional strain on sealant mechanics and adhesion. Although minimal data specifying the required adhesion strength for lung sealants are available, peak inspiratory pressure is often used to determine the maximum pressure that a sealant must be able to withstand. Peak inspiratory pressure is reported to range from 15 to 25 cm H_2O under normal conditions and can reach as high as 50 cm H_2O during coughing, corresponding to a desired maximum adhesion strength of ≈4900 N m^{-2}. Assuming an application area of 1 cm^2, the adhesive force of the sealant preparation with 0.01% tannic acid is 13500 N m^{-2}, which significantly exceeds the required adhesion strength.

Pleural wound healing is achieved through the proliferation and migration of mesothelial cells, which are mediated by growth factors, monocyte/macrophage signaling, and lung fibroblasts.[30,79,80] In contrast to available sealants, which do not promote pleural wound healing, the lung-mimetic sealant is formulated with matrikines, which are bioactive signals that are derived from decellularized lung extracellular matrix and can promote tissue repair. Proteomic profiling of the matrikines in the sealant reveals the presence of chemokines and growth factors, for example, fibroblast growth factors (bFGF) and insulin-like growth factor binding proteins, which have been shown to stimulate mesothelial cell proliferation in vitro.[55,57] The lung-mimetic sealant also contains matrikines derived from extracellular matrix components found in the visceral pleura and matrikines associated with lung repair, including collagens I, III, IV, VI, and multiple laminin isoforms.[30,34,81–83] Laminin subunit alpha 5, hyaluronan, heparan sulfate, and other related matrikines may provide additional benefits due to their involvement in visceral pleural development, pleural lubrication, and pleural wound healing.[43,84,85] Although no order-of-magnitude changes in gene expression are observed, monocytes exposed to lung matrikines in vitro significantly upregulate genes associated with an M2C-like macrophage phenotype (Figure 4C), indicative of reparative cellular activities such as extracellular matrix remodeling, angiogenesis, vascularization, and phagocytosis of cellular debris.[86,87] Further, genes upregulated by macrophages in response to sealant lung matrikines, including IL1B, PDGF, and VEGF, are known promoters of mesothelial cell proliferation and lung tissue repair; and therefore, may support pleural wound healing.[30,55–57,79,88] PDGF has also been shown to promote hyaluronan synthase activity and hyaluronan secretion in mesothelial cells, a critical function for the regulation of pleural fluid.[89]

This study had several notable limitations: sealant effects on cells of diseased origin were not investigated but represent an important and clinically-relevant assessment of the lung-mimetic sealant to promote healing in a diseased setting, as patients with pulmonary air leak often have underlying lung disease. Future studies should also investigate sealant biodegradation, effects on pleural mesothelial cells, long-term effects on tissue healing in vivo, comparative performance against standard of care, development of protocols for intraoperative use, and requirements for GMP-grade manufacturing.

4. Conclusion

This lung-mimetic hydrofoam sealant is, to our knowledge, the first to feature a combination of lung-mimetic physicomechanical and bioactive properties that can synergistically restore lung mechanics and promote reparative cellular responses. We envision that tissue-mimetic design principles can be similarly applied to develop other tissue-specific surgical sealants for indications in dermal, gastrointestinal, vascular, and/or other tissues.

5. Experimental Section

Experimental Design: The objective of this study was to apply engineering design principles to develop a lung-mimetic sealant to treat pulmonary air leak. Design criteria were pre-defined, and a range of sealant formulations was systematically tested to ensure design criteria were satisfied. To evaluate sealant efficacy, two animal models of pulmonary air leak (rat and swine) were utilized. The study was designed to require the minimum number of animals to demonstrate sealant efficacy.

Lung-Mimetic Sealant Preparation: Gelatin powder from porcine skin (G2500, Sigma) was dissolved in phosphate-buffered saline at 70 °C. Tannic acid (403040, Sigma) was dissolved in phosphate-buffered saline at room temperature. Tannic acid was added to the gelatin solution dropwise while stirring, and pH was adjusted to 8.5 with 1 M sodium hydroxide. The solution was mixed for 1 hour at 55 °C, and pH was maintained at 8.5. Throughout mixing, air was introduced to the solution to provide oxidized conditions for the chemical reaction between gelatin and tannic acid. Decellularized lung extracellular matrix-derived matrikines (ExMatrico, Xylyx Bio) were prepared according to manufacturer's instruction and added to the gelatin–tannic acid solution while mixing. Transglutaminase (Ajinomoto Activa RM) was dissolved in phosphate-buffered saline at 37 °C and added to the solution to initiate crosslinking. Alveolar-like air bubbles were generated by vortexing the solution with a homogenizer (Fisherbrand 850 Homogenizer) or injecting air bubbles into the solution with a syringe during gelation. Final ranges of concentrations, presented as %weight/volume (w/v) of sealant components, were: 10% gelatin; 0.01–1% tannic acid; 1–4% transglutaminase; and 0.01–0.2% lung matrikines.

Scanning Electron Microscopy: Samples were fixed in 2.5% glutaraldehyde (Electron Microscopy Sciences, 16120) at 25 °C for 1 h followed by overnight fixation at 4 °C, rinsed in 70% ethanol, frozen, and lyophilized. Samples were gold sputter coated and imaged using a scanning electron microscope (GeminiSEM 300; Zeiss) with an accelerating voltage of 5.0 kV.

Pore Size Calculations: Scanning electron microscopy and histology images were imported to ImageJ software (NIH) and converted to binary images (16-bit). The image scale was set according to the scale bar of the image. The structure and boundaries of pores were enhanced and

specified using the "Threshold" option. Pore size and porosity values were calculated using the "Analyze Particle" function.

Compression Testing: Samples were prepared by pouring sealant formulations into a cylindrical silicon mold (diameter: 2.4 cm, height: 1 cm). Compression testing was performed according to the D965-15 ASTM standard with an Instron machine (5965, load cell: 5 kN) at crosshead speed of 1 mm min^{-1} for one cycle. Elastic moduli were determined by calculating the slope of the stress–strain curve at different strain ranges (low: 0–0.05, medium: 0.30–0.35, and high: 0.45–0.50).

Tension Testing: Samples were prepared using dumbbell-shaped polydimethylsiloxane (PDMS) molds (length: 3 cm, width: 6 mm, and thickness: 5 mm). Tension testing was performed with an Instron machine (5965, load cell: 5 kN) at a crosshead speed of 5 mm min^{-1} for one cycle until failure. Elastic moduli of sealant formulations were determined by calculating the slope of the linear region of the stress–strain curves ($\sigma = E \times \epsilon$, where σ is stress, E is elastic modulus, and ϵ is strain). Elongation at break percentage was calculated using $(L - L_0) \times 100/L_0$, where L is length of the sample at failure (break) and L_0 is initial length. Sealant toughness was determined by calculating the area under the stress–strain curve during elongation to failure measurements.

Adhesion Force Measurement: As tannic acid served as the tissue adhesion promoter, an adhesion test was performed to evaluate the optimum tannic acid concentration in the sealant. A custom apparatus was constructed using a digital force gauge (Series 5, Mark-10), compression platen, and tensile grip to measure adhesion force (Figure 3F). Double-layered samples were prepared such that the top layer was comprised of gelatin (10%) and transglutaminase (4%), and the bottom layer was comprised of gelatin (10%), transglutaminase (2%), and a range of tannic acid concentrations (Figure 3G). A circular collagen sheet substrate commonly used for adhesion testing[10,90] was soaked in phosphate-buffered saline, blotted dry, and fixed to the bottom platen using glue (Krazy Glue, Max Bond Gel). A double-layered sample was then heated to 50 °C and placed on top of the collagen sheet. After 5 min, an upward force was applied to the top layer via the tensile grip, and the adhesion force was continuously measured with a digital force meter until detachment of the bottom layer from the collagen sheet. Adhesion forces were reported from the point at which the sealant detached from the collagen substrate.

Proteomic Profiling: Sealant composition was characterized through liquid chromatography–tandem mass spectrometry (LC–MS/MS) and multiplex protein profiling (Eve Technologies).

Human Primary Lung Fibroblasts: Lung fibroblasts (CC-2512, Lonza) were maintained in growth media (CC-3132, Lonza) in a humidified environment at 37 °C with 5% CO_2 and passaged at 80–90% confluency.

Biocompatibility: Lung fibroblasts were added to a 24-well plate, and 7-mm sealant punch biopsies were prepared and added to each well. Cells were supplied with 1 mL growth media. Sealant punch biopsies formulated with gelatin and transglutaminase were prepared across a range of lung matrikine concentrations (0–0.2% w/v).

Cell Viability: Live/Dead staining was performed according to manufacturer's instructions. Briefly, Live/Dead reagent (2 µM calcein AM, 4 µM ethidium homodimer 1) was prepared fresh, added directly to cells, and incubated at 37 °C for 45 min. Cells were imaged using a fluorescence microscope (Olympus IX81) with excitation/emission of 494/517 nm (calcein AM) and 528/617 nm (ethidium homodimer 1). The images were processed using ImageJ.

Cytotoxicity: PrestoBlue reagent (ThermoFisher, A13261) was diluted 1:10 in growth media, added to cells co-cultured with sealant formulations, and incubated for 10 min at 37 °C with 5% CO_2. Supernatants were transferred to a 24 well-plate, and fluorescence was measured on a plate reader with excitation/emission of 530/590 nm.

Isolation and Culture of HumanPrimary Monocytes: Monocytes were isolated via negative selection from enriched human peripheral blood leukopaks (New York Blood Center) using an EasySep Direct Human Monocyte Isolation Kit (StemCell Tech), according to manufacturer's instructions. Leukopaks were diluted in an equal volume of 6 mM EDTA to yield a final concentration of 3 mM EDTA prior to immunomagnetic negative selection. Isolated CD14+ monocytes were frozen in CryoStor cryopreservation media and stored in liquid nitrogen until use.

Immunogenicity: Monocytes were cultured overnight in 24-well ultra-low attachment tissue culture plates at a concentration of 1×10^6 cells per well in RPMI 1640 media supplemented with 10% human serum, 1% penicillin streptomycin, and 20 ng mL^{-1} macrophage colony-stimulating factor. Transwell inserts (0.4 µm pore size, Corning, 3470) containing 7-mm punch biopsies of lung sealant formulations across a range of matrikine concentrations (0%, 0.01%, 0.05%, 0.1%, and 0.2% w/v) were subsequently added to each well for non-contact immunogenicity characterization. Monocytes were cultured in the absence of lung sealant, and lung sealant without monocytes served as controls. On day 3 of transwell co-culture, inserts containing lung sealant were transferred to new 24-well plates and frozen at −80 °C. Supernatant from the basolateral chamber was centrifuged at 300 × *g* for 5 min and stored at −80 °C for protein analysis. Monocytes were lysed in 350 µL Buffer RLT and stored at −80 °C until RNA isolation.

RNA Isolation, cDNA Synthesis, and RT-PCR: RNA was isolated using RNeasy Micro Kit (Qiagen, 74004) according to manufacturer's instructions, with on-column digestion of genomic DNA. RNA was eluted into 14 µL RNase-free water and quantified using a NanoDrop One Spectrophotometer (Thermo Fisher Scientific). RNA was considered pure if the ratio of absorbance at 260/280 nm was ≥ 2. cDNA was synthesized from 1 µg RNA using a High-Capacity cDNA Reverse Transcription Kit (Applied Biosystems) and stored at −80 °C. Quantitative RT-PCR was performed using 20 ng cDNA and Fast SYBR Green Master Mix (Applied Biosystems), according to manufacturer's instructions. Mean quantification cycle, Cq, values were calculated from technical replicates. Expression of target genes was normalized to the reference gene GAPDH. All primers (Table S3, Supporting Information) were synthesized by Life Technologies.

Sealant Application in Rat Lungs: All rat procedures were performed in accordance with the animal welfare guidelines and regulations of the Institute for Animal Care and Use Committee (IACUC) at the Stevens Institute of Technology. Rats ($n = 5$, Sprague–Dawley, 200–250 g, Charles River Laboratories) were anesthetized via inhalation of 2.5% isoflurane for 10 min in an induction chamber using a vaporizer (SomnoSuite, Kent Scientific). To prevent clotting in the lung, 0.5 mL of 1000 U mL^{-1} heparin was injected into the tail vein. A midline laparotomy was performed, and the animal was euthanized by transection of the inferior vena cava, leading to exsanguination. To cannulate the trachea, an incision was made cranially past the manubrium into the neck. An endotracheal tube (diameter: 2 mm; 73–2727, Harvard Apparatus) was inserted and secured with a suture (size: 4.0, Matrix Wizard). A small animal ventilator (PhysioSuite, Kent Scientific) was used to ventilate the lungs at a tidal volume of 2.2 mL, respiratory rate of 70 breaths per min, and positive end-expiratory pressure (PEEP) of 2.2 cm H_2O. A midline thoracotomy was then performed to open the chest and expose the lungs. An injury (2 cm) was created using scissors to induce air leak, and sealant (gelatin: 10%, transglutaminase: 2%, tannic acid: 0.1%, lung matrikines: 0.012%) was applied to the site of air leak. Airway pressure, volumes of inspiration and expiration, and pressure–volume curves were obtained from the ventilator and pressure and flow sensors integrated in the ventilation tubing. Lungs were compared at baseline, after air leak, and after sealant application.

Sealant Application in Ex Vivo Swine Lungs: Swine lungs were explanted in standard fashion, intubated with an endotracheal tube (size: 7.5 mm), and connected to a ventilator (Oxylog 3000 plus, Dräger) with the following settings: volume control mode, respiratory rate, 6–8 breaths per min; tidal volume, 10–12 mL kg^{-1}; PEEP, 5 cm H_2O; and 40% FiO_2. Pulmonary air leak was induced by a focal puncture through the visceral pleura using an 18G needle. Tidal volumes and ventilation parameters were monitored. To confirm the presence of air leak, the site of air leak was submerged in normal saline, and air bubbles were visualized. Following submersion in normal saline, the surface of the pleura was then gently patted with gauze to remove excess saline. Lung-mimetic sealant was administered (2 mL per application) using a 22G needle through the injured pleura;while, lung ventilation was held to mimic intraoperative application. Following sealant application, the treated site was submerged in normal saline to assess for visible air bubbles.

Quantitative Sound Analysis: Quantitative sound analysis algorithms were used to detect presence or absence of air leak in swine lungs, as

previously described.[69] Measurements were performed at baseline, after air leak induction, and after sealant application, and analyzed using Audacity and custom MATLAB code. Values were averaged across three breaths.

Histology: Sealant application sites were resected with a surgical stapler, fixed in 4% phosphate-buffered paraformaldehyde at 4 °C for 24 h, paraffin-embedded, sectioned, and mounted on glass slides. Slides were stained with hematoxylin and eosin (H&E) and imaged using a slide scanner (SCN400, Leica) at 20×. Histological staining was performed by the core service in the Department of Molecular Pathology at Columbia University Medical Center.

Statistical Analysis: All data are presented as mean ± standard deviation. One-way ANOVA followed by Tukey's honest significant post hoc test was used to perform multiple comparisons, and *t*-test was used to evaluate differences between groups. Statistical significance was indicated for $p < 0.05$. All measurements were repeated at least three times.

Supporting Information

Supporting Information is available from the Wiley Online Library or from the author.

Acknowledgements

The authors thank the following collaborators and supporters: Herbert Irving Comprehensive Cancer Center Molecular Pathology Shared Resources Facility at Columbia University, especially S. Dajiang and T. Wu; the Columbia Biomedical Engineering Technology Accelerator (BiomedX) Oversight Committee, especially K. Reuther, for guidance on project development; Columbia University Institute of Comparative Medicine, especially A. Romanov, M. Kain, and M. Morris, for oversight of large animal studies; and S. Halligan, K. Cunningham, and A. Grossbarth for administrative and logistical support. The authors gratefully acknowledge funding support from the Columbia Biomedical Engineering Technology Accelerator (BiomedX), Columbia Technology Ventures (CTV Validation Fund to G.V.-N.), National Institutes of Health (Grants EB027062, HL134760, HL120046), National Science Foundation (CAREER Award 2143620 to J.K.), and the New Jersey Health Foundation (PC 5–21 to J.K.).

Conflict of Interest

M.R.P., B.A.G., J.D.O., M.B., J.K., and G.V-N. are co-inventors on a patent (US11291747B2) describing the lung-mimetic sealant. J.D.O. is an officer of Xylyx Bio, Inc., a supplier of extracellular matrix biomaterials. J.D.O., M.B., and G.V-N. own stock in Xylyx Bio, Inc.

Author Contributions

M.R.P. and M.M. contributed equally to this work. M.R.P., M.M., B.A.G., J.D.O., M.B., J.K., and G.V-N. contributed to conceptualization: M.R.P., M.M., P.L.G., D.N.T., and M.H. contributed to methodology. M.R.P., M.M., P.L.G., D.N.T., J.C., M.H., O.G., P.C., S.R.K., J.A.R., and J.V.H. contributed to experimentation. M.R.P., M.M., P.L.G., D.N.T., J.C., and J.K. contributed to data analysis. M.R.P., M.M., J.D.O., and J.K. contributed to data visualization. B.A.G., J.D.O., M.B., J.K., and G.V-N. contributed to supervision. M.R.P., M.M., J.D.O., and J.K. contributed to manuscript production. P.L.G., D.N.T., J.C., M.H., O.G., P.C., S.R.K., J.A.R., J.V.H., B.A.G., J.D.O, M.B., J.K., and G.V.-N. contributed to manuscript review. J.K. and G.V-N. contributed to funding.

Data Availability Statement

The data that support the findings of this study are available from the corresponding author upon reasonable request.

Keywords

thoracic surgery, lung extracellular matrix, pneumothorax, biomimetic materials

Received: September 10, 2023
Revised: December 22, 2023
Published online: February 14, 2024

[1] M. R. Mueller, B. A. Marzluf, *J. Thorac. Dis.* **2014**, *6*, 271.
[2] K. C. Dugan, B. Laxmanan, S. Murgu, D. K. Hogarth, *Chest* **2017**, *152*, 417.
[3] R. M. Mercer, M. Hassan, N. M. Rahman, *Expert Rev. Respir. Med.* **2018**, *12*, 323.
[4] R. Kawachi, R. Matsuwaki, K. Tachibana, S. Karita, Y. Nakazato, R. Tanaka, Y. Nagashima, H. Takei, H. Kondo, *Interact. Cardiovasc. Thorac. Surg.* **2016**, *23*, 190.
[5] E. Okur, A. Kir, S. Halezeroglu, A. L. Alpay, A. Atasalihi, *Eur. J. Cardio-Thorac. Surg.* **2001**, *20*, 1012.
[6] I. Gakidis, *Med. Sci. Monit.* **2015**, *21*, 432.
[7] Y. H. Yang, S. Y. Park, H. E. Kim, B. J. Park, C. Y. Lee, J. G. Lee, D. J. Kim, H. C. Paik, *Thoracic Cancer* **2022**, *13*, 1401.
[8] R. C. Gologorsky, A. L. Alabaster, S. K. Ashiku, A. R. Patel, J. B. Velotta, *Perm. J.* **2019**, *23*, 18.
[9] J. Belda-Sanchís, M. Serra-Mitjans, M. Iglesias Sentis, R. Rami, *Cochrane Database Syst. Rev.* **2010**, *2010*, CD003051.
[10] A. Assmann, A. Vegh, M. Ghasemi-Rad, S. Bagherifard, G. Cheng, E. S. Sani, G. U. Ruiz-Esparza, I. Noshadi, A. Lassaletta, S. Gangadharan, A. Tamayol, A. Khademhosseini, N. Annabi, *Biomaterials* **2017**, *140*, 115.
[11] F. Zaraca, M. Vaccarili, G. Zaccagna, P. Maniscalco, G. Dolci, B. Feil, R. Perkmann, L. Bertolaccini, R. Crisci, *J. Thorac. Dis.* **2017**, *9*, 5230.
[12] K. D. Mortman, M. Corral, X. Zhang, I. Berhane, I. M. Soleas, N. C. Ferko, *J. Med. Econ.* **2018**, *21*, 1016.
[13] D. F. Torchiana, *J. Card. Surg.* **2003**, *18*, 504.
[14] A. M. Gillinov, B. W. Lytle, *J. Card. Surg.* **2001**, *16*, 255.
[15] T. B. Pedersen, J. L. Honge, H. K. Pilegaard, J. M. Hasenkam, *Ann. Thorac. Surg.* **2012**, *94*, 234.
[16] M. G. Cravens, A. W. Behn, J. L. Dragoo, *Clin. Biomech.* **2017**, *49*, 34.
[17] R. Zhang, M. Bures, K. Höffler, D. Jonigk, A. Haverich, M. Krueger, *Thorac. Cardiovasc. Surg.* **2014**, *62*, 705.
[18] M. Bures, H. K. Höffler, G. Friedel, T. Kyriss, E. Boedeker, F. Länger, P. Zardo, R. Zhang, *J. Cardiothorac. Surg.* **2016**, *11*, 63.
[19] H. H. Chao, D. F. Torchiana, *J. Card. Surg.* **2003**, *18*, 500.
[20] M. M. Joglekar, D. J. Slebos, J. Leijten, J. K. Burgess, S. D. Pouwels, *Eur. Respir. Rev.* **2021**, *30*, 210142.
[21] C. N. Grover, R. E. Cameron, S. M. Best, *J. Mech. Behav. Biomed. Mater.* **2012**, *10*, 62.
[22] J. Guo, W. Sun, J. P. Kim, X. Lu, Q. Li, M. Lin, O. Mrowczynski, E. B. Rizk, J. Cheng, G. Qian, J. Yang, *Acta Biomater.* **2018**, *72*, 35.
[23] Q. Zhao, S. Mu, Y. Long, J. Zhou, W. Chen, D. Astruc, C. Gaidau, H. Gu, *Macromol. Mater. Eng.* **2019**, *304*, 1800664.
[24] A. Schestakow, M. S. Guth, T. A. Eisenmenger, M. Hannig, *Molecules* **2021**, *26*, 1351.
[25] G. Yang, Z. Xiao, H. Long, K. Ma, J. Zhang, X. Ren, J. Zhang, *Sci. Rep.* **2018**, *8*, 1616.
[26] C. W. Yung, L. Q. Wu, J. A. Tullman, G. F. Payne, W. E. Bentley, T. A. Barbari, *J. Biomed. Mater. Res. A* **2007**, *83*, 1039.
[27] J. Chen, S. M. Mir, M. R. Pinezich, J. D. O'Neill, B. A. Guenthart, M. Bacchetta, G. Vunjak-Novakovic, S. X. L. Huang, J. Kim, *Acta Biomater.* **2021**, *131*, 370.

[28] M. R. Pinezich, M. A. Tamargo, S. Fleischer, J. A. Reimer, M. R. Hudock, A. E. Hozain, S. R. Kaslow, Y. Tipograf, R. K. Soni, O. P. Gavaudan, B. A. Guenthart, C. C. Marboe, M. Bacchetta, J. D. O'Neill, N. V. Dorrello, *J. Cyst. Fibros.* **2022**, *21*, 1027.
[29] L. Liu, B. Stephens, M. Bergman, A. May, T. Chiang, *Bioengineering* **2021**, *8*, 13.
[30] R. M. Davila, E. C. Crouch, *Am. J. Pathol.* **1993**, *142*, 547.
[31] G. Jolles, R.-P. R. Ltd, *T-lymphocyte and inflammatory cell research in asthma*, Academic Press, London, **1993**. 376 p.
[32] R. G. Marangoni, B. D. Korman, E. R. Parra, A. P. P. Velosa, H. V. Barbeiro, V. Martins, A. B. G. Dos Santos, F. Soriano, W. R. Teodoro, P. L. Silva, W. Tourtellotte, V. L. Capelozzi, J. Varga, N. H. Yoshinari, *Pathol., Res. Pract.* **2021**, *220*, 153382.
[33] T. L. Sumpter, D. S. Wilkes, *Am. J. Physiol.: Lung Cell. Mol. Physiol.* **2004**, *286*, L1129.
[34] J. A. Mereness, S. Bhattacharya, Q. Wang, Y. Ren, G. S. Pryhuber, T. J. Mariani, *PLoS One* **2018**, *13*, e0209095.
[35] Y. Muragaki, M. G. Mattei, N. Yamaguchi, B. R. Olsen, Y. Ninomiya, *Eur. J. Biochem.* **1991**, *197*, 615.
[36] P. Parsons, S. J. Gilbert, A. Vaughan-Thomas, D. A. Sorrell, R. Notman, M. Bishop, A. J. Hayes, D. J. Mason, V. C. Duance, *J. Biol. Chem.* **2011**, *286*, 34986.
[37] Z. Raglow, S. M. Thomas, *Cancer Lett.* **2015**, *357*, 448.
[38] S. Grässel, R. J. Bauer, *Matrix Biol.* **2013**, *32*, 64.
[39] B. Mariko, Z. Ghandour, S. Raveaud, M. Quentin, Y. Usson, J. Verdetti, P. Huber, C. Kielty, G. Faury, *Am. J. Physiol.: Cell Physiol.* **2010**, *299*, C977.
[40] M. Fricke, C. Langer, E. Brunner, L. Y. Sakai, L. Füzesi, D. P. Reinhardt, F. Quondamatteo, *J. Anat.* **2008**, *212*, 674.
[41] M. J. Lee, N. K. Roy, J. E. Mogford, W. P. Schiemann, T. A. Mustoe, *J. Am. Coll. Surg.* **2004**, *199*, 403.
[42] Y. Hirai, Y. Muragaki, S. Itoh, K. Oikawa, M. Juri, T. Kondo, Y. Okamura, *Ann. Thorac. Cardiovasc. Surg.* **2012**, *18*, 200.
[43] N. M. Nguyen, J. H. Miner, R. A. Pierce, R. M. Senior, *Dev. Biol.* **2002**, *246*, 231.
[44] P. L. Durham, J. M. Snyder, *Differentiation* **1996**, *60*, 229.
[45] P. Ekblom, M. Ekblom, L. Fecker, G. Klein, H. Y. Zhang, Y. Kadoya, M. L. Chu, U. Mayer, R. Timpl, *Development* **1994**, *120*, 2003.
[46] K. M. Akram, S. Samad, M. A. Spiteri, N. R. Forsyth, *Respir. Res.* **2013**, *14*, 9.
[47] K. Izuhara, S. J. Conway, B. B. Moore, H. Matsumoto, C. T. J. Holweg, J. G. Matthews, J. R. Arron, *Am J. Respir. Crit. Care Med.* **2016**, *193*, 949.
[48] L. W. Place, M. Sekyi, M. J. Kipper, *Biomacromolecules* **2014**, *15*, 680.
[49] M. C. Farach-Carson, C. R. Warren, D. A. Harrington, D. D. Carson, *Matrix Biol.* **2014**, *34*, 64.
[50] S. P. Evanko, M. D. Gooden, I. Kang, C. K. Chan, R. B. Vernon, T. N. Wight, *J. Histochem. Cytochem.* **2020**, *68*, 797.
[51] M. Lausen, N. Lynch, A. Schlosser, I. Tornoe, S. G. Saekmose, B. Teisner, A. C. Willis, E. Crouch, W. Schwaeble, U. Holmskov, *J. Biol. Chem.* **1999**, *274*, 32234.
[52] J. A. Poole, T. M. Nordgren, A. J. Heires, A. J. Nelson, D. Katafiasz, K. L. Bailey, D. J. Romberger, *Am. J. Physiol.: Lung Cell. Mol. Physiol.* **2020**, *318*, L180.
[53] B. Banan, R. Watson, M. Xu, Y. Lin, W. Chapman, *Liver Transplant.* **2016**, *22*, 979.
[54] S. Ogata-Suetsugu, T. Yanagihara, N. Hamada, C. Ikeda-Harada, T. Yokoyama, K. Suzuki, T. Kawaguchi, T. Maeyama, K. Kuwano, Y. Nakanishi, *Biochem. Biophys. Res. Commun.* **2017**, *484*, 422.
[55] S. E. Mutsaers, R. J. McAnulty, G. J. Laurent, M. A. Versnel, D. Whitaker, J. M. Papadimitriou, *Eur. J. Cell Biol.* **1997**, *72*, 24.
[56] E. W. Gabrielson, B. I. Gerwin, C. C. Harris, A. B. Roberts, M. B. Sporn, J. F. Lechner, *FASEB J.* **1988**, *2*, 2717.
[57] M. A. Laveck, A. N. A. Somers, L. L. Moore, B. I. Gerwin, J. F. Lechner, *In Vitro Cell. Dev. Biol.* **1988**, *24*, 1077.
[58] C. A. Guenther, Z. Wang, E. Li, M. C. Tran, C. Y. Logan, R. Nusse, L. Pantalena-Filho, G. P. Yang, D. M. Kingsley, *Bone* **2015**, *77*, 31.
[59] L. C. C. Yeh, *Int. J. Biomed. Sci.* **2010**, *6*, 176.
[60] R. A. M. Panganiban, R. M. Day, *Acta Pharmacol. Sin.* **2011**, *32*, 12.
[61] A. Gazdhar, P. Fachinger, C. van Leer, J. Pierog, M. Gugger, R. Friis, R. A. Schmid, T. Geiser, *Am. J. Physiol.: Lung Cell. Mol. Physiol.* **2007**, *292*, L529.
[62] W. L. Stuard, R. Titone, D. M. Robertson, *FASEB J.* **2022**, *36*, e22062.
[63] R. Muterspaugh, D. Price, D. Esckilsen, S. McEachern, J. Guthrie, D. Heyl, H. G. Evans, *Biochemistry* **2018**, *57*, 5726.
[64] G. Dahlfors, H. J. Arnqvist, *Endocrinology* **2000**, *141*, 2062.
[65] Z. Wang, Y. Qi, R. Wang, W. Wu, Z. Li, M. Wang, R. Liu, C. Zhang, W. Li, S. Wang, *J. Cell. Physiol.* **2020**, *235*, 9538.
[66] E. Ehrenborg, H. Zazzi, S. Lagercrantz, M. Granqvist, U. Hillerbrand, S. V. Allander, C. Larsson, H. Luthman, *Mamm. Genome* **1999**, *10*, 376.
[67] C. Gemelli, A. Grande, S. Ferrari, A. Tomasi, A. Cuoghi, *Eur. J. Inflamm.* **2019**, *17*, 205873921882047.
[68] N. Jariwala, M. Ozols, M. Bell, E. Bradley, A. Gilmore, L. Debelle, M. J. Sherratt, *Adv. Drug Delivery Rev.* **2022**, *185*, 114240.
[69] M. R. Pinezich, S. M. Mir, J. A. Reimer, S. R. Kaslow, J. Chen, B. A. Guenthart, M. Bacchetta, J. D. O'Neill, G. Vunjak-Novakovic, J. Kim, *Bioeng. Transl. Med.* **2023**, *8*, e10322.
[70] E. Roan, C. M. Waters, *Am. J. Physiol.: Lung Cell. Mol. Physiol.* **2011**, *301*, L625.
[71] D. J. Finley, V. W. Rusch, *Thorac. Surg. Clin.* **2011**, *21*, 157.
[72] E. D'Angelo, S. H. Loring, M. E. Gioia, M. Pecchiari, C. Moscheni, *Respir. Physiol. Neurobiol.* **2004**, *142*, 55.
[73] A. G. Markov, S. Amasheh, *Front. Physiol.* **2014**, *5*, 221.
[74] S. J. Li, K. Zhou, Y. M. Wu, M. M. Wang, C. Shen, Z. Q. Wang, G. W. Che, L. X. Liu, *J. Thorac. Dis.* **2018**, *10*, 416.
[75] G. W. H. van, K. Klooster, J. E. Hartman, N. Hacken, H. A. M. Kerstjens, R. F. E. Wolf, D. J. Slebos, *J. Reticuloendothel. Soc.* **2017**, *94*, 224.
[76] M. A. Gwak, B. M. Hong, J. M. Seok, S. A. Park, W. H. Park, *Int. J. Biol. Macromol.* **2021**, *191*, 699.
[77] S. J. Lee, M. A. Gwak, K. Chathuranga, J. S. Lee, J. Koo, W. H. Park, *Food Hydrocolloids* **2023**, *136*, 108249.
[78] S. Rivero, M. A. García, A. Pinotti, *Carbohydr. Polym.* **2010**, *82*, 270.
[79] S. E. Mutsaers, *Respirology* **2002**, *7*, 171.
[80] Z. Fotev, D. Whitaker, J. M. Papadimitriou, *J. Pathol.* **1987**, *151*, 209.
[81] S. I. Rennard, M. C. Jaurand, J. Bignon, O. Kawanami, V. J. Ferrans, J. Davidson, R. G. Crystal, *Am. Rev. Respir. Dis.* **1984**, *130*, 267.
[82] S. J. Hwang, G. H. Ha, W. Y. Seo, C. K. Kim, K. Kim, S. B. Lee, *BMB Rep.* **2020**, *53*, 539.
[83] D. M. Hoganson, G. E. Owens, E. M. O'Doherty, C. M. Bowley, S. M. Goldman, D. O. Harilal, C. M. Neville, R. T. Kronengold, J. P. Vacanti, *Biomaterials* **2010**, *31*, 6934.
[84] N. M. Nguyen, R. M. Senior, *Dev. Biol.* **2006**, *294*, 271.
[85] P. Olczyk, Ł. Mencner, K. Komosinska-Vassev, *BioMed Res. Int.* **2015**, *2015*, 549417.
[86] P. L. Graney, S. Ben-Shaul, S. Landau, A. Bajpai, B. Singh, J. Eager, A. Cohen, S. Levenberg, K. L. Spiller, *Sci. Adv.* **2020**, *6*, eaay6391.
[87] Y. Yao, X. H. Xu, L. Jin, *Front. Immunol.* **2019**, *10*, 792.
[88] L. M. Crosby, C. M. Waters, *Am. J. Physiol.: Lung Cell Mol. Physiol.* **2010**, *298*, L715.
[89] P. Heldin, T. Asplund, D. Ytterberg, S. Thelin, T. C. Laurent, *Biochem. J.* **1992**, *283*, 165.
[90] D. G. Wallace, G. M. Cruise, W. M. Rhee, J. A. Schroeder, J. J. Prior, J. Ju, M. Maroney, J. Duronio, M. H. Ngo, T. Estridge, G. C. Coker, *J. Biomed. Mater. Res.* **2001**, *58*, 545.